Conditions for tidal bore formation in convergent alluvial estuaries

Philippe Bonneton [a, *], Andrea Gilberto Filippini [b], Luca Arpaia [b], Natalie Bonneton [a], Mario Ricchiuto [b]

[a] CNRS, UMR EPOC, University of Bordeaux, Talence, France
[b] Team CARDAMOM, INRIA Bordeaux Sud-Ouest, Institut de Mathématiques de Bordeaux, France

ABSTRACT

Over the last decade there has been an increasing interest in tidal bore dynamics. However most studies have been focused on small-scale bore processes. The present paper describes the first quantitative study, at the estuary scale, of the conditions for tidal bore formation in convergent alluvial estuaries. When freshwater discharge and large-scale spatial variations of the estuary water depth can be neglected, tide propagation in such estuaries is controlled by three main dimensionless parameters: the nonlinearity parameter ε_0, the convergence ratio δ_0 and the friction parameter ϕ_0. In this paper we explore this dimensionless parameter space, in terms of tidal bore occurrence, from a database of 21 estuaries (8 tidal-bore estuaries and 13 non tidal-bore estuaries). The field data point out that tidal bores occur for convergence ratios close to the critical convergence δ_c. A new proposed definition of the friction parameter highlights a clear separation on the parameter plane (ϕ_0, ε_0) between tidal-bore estuaries and non tidal-bore estuaries. More specifically, we have established that tidal bores occur in convergent estuaries when the nonlinearity parameter is greater than a critical value, ε_c, which is an increasing function of the friction parameter ϕ_0. This result has been confirmed by numerical simulations of the two-dimensional Saint Venant equations. The real-estuary observations and the numerical simulations also show that, contrary to what is generally assumed, tide amplification is not a necessary condition for tidal bore formation. The effect of freshwater discharge on tidal bore occurrence has been analyzed from the database acquired during three long-term campaigns carried out on the Gironde/Garonne estuary. We have shown that in the upper estuary the tidal bore intensity is mainly governed by the local dimensionless tide amplitude ε. The bore intensity is an increasing function of ε and this relationship does not depend on freshwater discharge. However, freshwater discharge damps the tidal wave during its propagation and thus reduces ε and consequently limits the tidal bore development in the estuary. To take into account this process in the tidal-bore scaling analysis, it is necessary to introduce a fourth external parameter, the dimensionless river discharge $\mathcal{Q}_0$.

© 2016 Elsevier Ltd. All rights reserved.

1. Introduction

Tidal bores are an intense nonlinear wave phenomenon which has been observed in many convergent alluvial estuaries worldwide (see example in Fig. 1). Up until the beginning of the 21st century, tidal bore characterization in natural environments was based essentially on qualitative observations (see Lynch (1982) and Bartsch-Winkler and Lynch (1988)). In the last decade several quantitative field studies have been devoted to the analysis of wave, turbulent and sediment processes associated with tidal bores (e.g. (Simpson et al., 2004; Wolanski et al., 2004; Uncles et al., 2006; Bonneton et al., 2011a, 2012; Chanson et al., 2011; Furgerot et al., 2013)). Most of these studies focused on well-developed tidal bores and small scale processes for some specific estuaries, but not on the tidal-bore occurrence conditions for any given alluvial estuaries.

The basic conditions for tidal bore formation are well-known (Bartsch-Winkler and Lynch (1988)): a large tidal range, a shallow and convergent channel, and low freshwater discharge. Yet, estuarine classification in terms of tidal bore occurrence cannot be

Fig. 1. Illustration of a tidal bore propagating in the Garonne River. Aerial photograph taken at Podensac on September 10, 2010. Tidal wave amplitude at the estuary mouth $A_0 = 2.5$ m and freshwater discharge $q_0 = 128$ m³/s.

established from simple criteria based on these hydrodynamic and geometric conditions. Nevertheless, bore formation criteria based on the tidal range, Tr, has been published (Bartsch-Winkler and Lynch (1988) and Chanson (2012)). For instance, in his numerous publications, *Chanson* asserts that *a tidal bore forms when the tidal range exceeds 4–6 m and the flood tide is confined to a narrow funneled estuary*. The tidal range used in this empirical criterion is not clearly defined. Thus, the criterion was tested based on two different definitions. Firstly, we defined the tidal range as the one at the estuary mouth Tr_0. In this case, field observations do not support the empirical criterion proposed by Chanson. For instance, Furgerot (2014) showed that in the Sée/Mont Saint Michel estuary, Tr_0 must be larger than 10 m for tidal bore formation and, on the other hand, Bonneton et al. (2015) observed tidal bores in the Gironde/Garonne estuary for Tr_0 smaller than 2 m. Alternatively, we consider a local tidal range Tr at a location in the estuary where tidal bore can form. Once again field observations do not support the Tr-criterion. For instance, Bonneton et al. (2012) showed that in the Seine estuary the local tidal range must be greater than 8 m for bore formation and, on the other hand, Furgerot et al. (2013) observed tidal bores in the Sée River when $Tr = 1$ m. These examples prove that such a simple criterion, based on a dimensional flow variable, cannot be relevant to determine tidal bore occurrence.

The objective of the present study is to analyze the conditions which control tidal bore formation in convergent alluvial estuaries. We develop a scaling analysis of the global tidal wave transformation as a function of both the tidal forcing at the estuary mouth and the large-scale geometric properties of the channel. From this analysis we proposed an estuarine classification, in terms of tidal bore occurrence, as a function of several dimensionless parameters.

2. Scaling analysis

A tidal bore can form when a large-amplitude tidal-wave propagates upstream a long shallow alluvial estuary. This large-scale tidal-wave transformation is largely controlled by a competition between bottom friction, channel convergence and freshwater discharge (e.g. Friedrichs (2010), Savenije (2012)). To determine the conditions favorable to tidal bore occurrence, a scaling analysis of this complex physical problem is required. Although such an analysis is common to study tidal wave propagation in estuaries (e.g. LeBlond (1978), Parker (1991), Friedrichs and Aubrey (1994), Lanzoni and Seminara (1998), Toffolon et al. (2006), Savenije et al. (2008)), only few studies have addressed tidal bore formation (Munchow and Garvine (1991) and Bonneton et al. (2015)). Thus, this paper aims to fill in this gap of research by clarifying which dimensionless parameters effectively control tidal bore occurrence in alluvial estuaries.
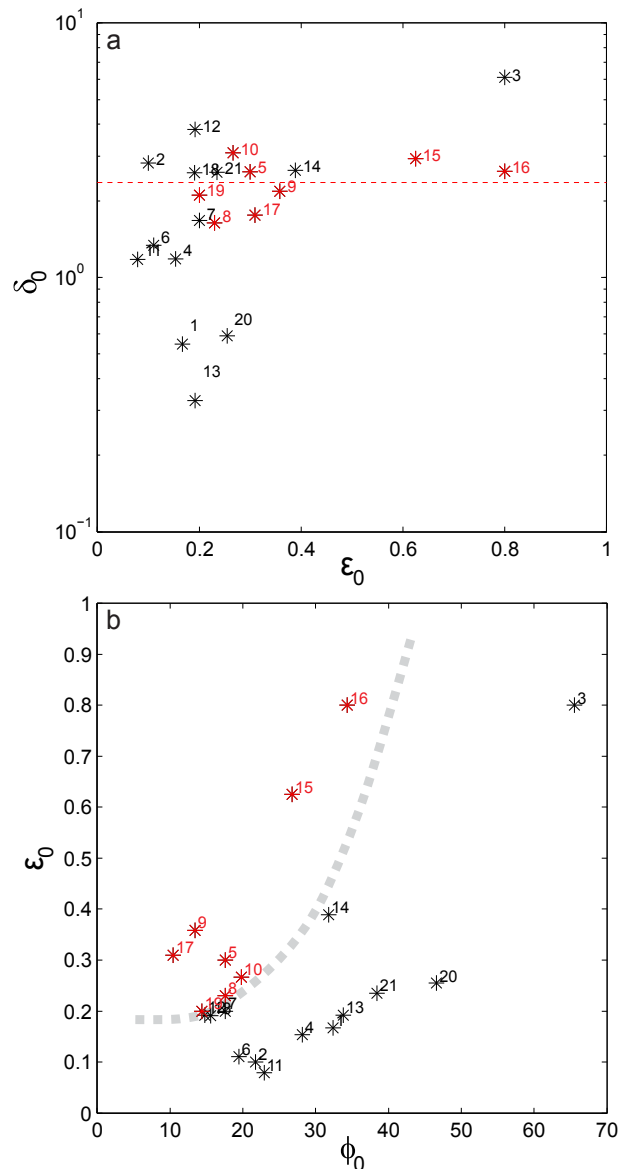

Fig. 2. Position of convergent alluvial estuaries (see Table 1) in the parameter space (ε_0, δ_0, ϕ_0). Red and black asterisks correspond to estuaries with and without tidal bore respectively. a, projection on the plane (ε_0, δ_0). The red dashed line corresponds to the mean value of δ_0 for the 8 tidal-bore estuaries; b, projection on the plane (ϕ_0, ε_0). The thick dashed line ($\varepsilon_c = f(\phi_0)$) divides the plane into two estuarine regimes: estuaries with and without tidal bore. This dashed line was drawn by eye and by drawing on the trend observed in Fig. 4. (For interpretation of the references to colour in this figure legend, the reader is referred to the web version of this article.)

Alluvial estuaries are characterized by movable beds made of sediments of riverine and marine origin. The shape of such estuaries is the result of feedback mechanisms between the flow field and the sediment transport processes. In tide-dominated environments, the self-formed tidal channels are generally funnel shaped with a width that tapers upstream in an approximately exponential fashion and with a fairly horizontal bottom (see Lanzoni and Seminara (1998), Davies and Woodroffe (2010), Savenije (2012)). Thus, an alluvial estuary geometry can generally be characterized by two characteristic length scales: the mean water depth D_0 and the convergence length L_{b0}, which is defined by

$L_{b0} = \left| B / \frac{dB}{dx} \right|$, where $B(x)$ is the channel width and x is the along-channel coordinate. It is worth noting that our scaling analysis does not describe possible large-scale spatial variations of the estuary water depth.

The forcing tidal wave at the estuary mouth can be characterized by its period T_0 and its amplitude $A_0 = Tr_0/2$, where Tr_0 is the tidal range. Most intense tidal bores occur during spring tides and low freshwater discharge periods. It is thus appropriate to choose the mean spring tidal amplitude at the estuary mouth as the characteristic amplitude A_0, and to neglect, as a first step, freshwater discharge effects on tidal wave dynamics. Another important parameter which controls tide propagation in the estuary is the friction coefficient (e.g. *LeBlond* (LeBlond, 1978), Parker (1991), Friedrichs and Aubrey (1994), Lanzoni and Seminara (1998)). Following Lanzoni and Seminara (1998) and many other authors we consider for each estuary a characteristic and constant friction coefficient, C_{f0}, representative of the whole estuary.

From the external variables of the problem, D_0, T_0, A_0, L_{b0} and C_{f0}, we will perform a scaling analysis of the flow equations. Our analysis focuses on the large scale tidal wave transformation which can lead locally to tidal bore formation. For such a large scale analysis, the small scale nonhydrostatic effects, associated with tidal bores (Bonneton et al. (2011b) and Bonneton et al. (2015)), can be neglected. Thus, the relevant tidal flow equations are the cross-sectionally integrated Saint Venant equations. For a horizontal bottom and an exponentially decreasing channel width, these equations may be expressed as:

$$\frac{\partial \zeta}{\partial t} + u \frac{\partial \zeta}{\partial x} + D \frac{\partial u}{\partial x} - \frac{uD}{L_{b0}} = 0 \tag{1}$$

$$\frac{\partial u}{\partial t} + u \frac{\partial u}{\partial x} + g \frac{\partial \zeta}{\partial x} + C_{f0} \frac{|u|u}{D} = 0, \tag{2}$$

where ζ is the surface elevation, D the cross-sectionally averaged water depth, u the cross-sectionally averaged velocity and g the gravity.

We introduce the following scaling:

$$x = L_0 x', \; t = \omega_0^{-1} t', \; D = D_0 D', \; \zeta = A_0 \zeta', \; u = U_0 u',$$

where $\omega_0 = 2\pi/T_0$ is the angular tidal frequency and U_0 and L_0 are the scales of velocity and length, respectively. The two later variables cannot be prescribed a priori since they depend on the channel response to a given forcing. U_0 and L_0 are functions of the external variables.

The dimensionless equations of motion may be expressed as (after dropping the primes for the sake of clarity):

$$\frac{\partial \zeta}{\partial t} + \frac{K}{\mathcal{L}} \left(\epsilon_0 u \frac{\partial \zeta}{\partial x} + D \frac{\partial u}{\partial x} \right) - KuD = 0 \tag{3}$$

$$\frac{\partial u}{\partial t} + \frac{K}{\mathcal{L}} \epsilon_0 u \frac{\partial u}{\partial x} + \frac{1}{K\mathcal{L}} \delta_0^2 \frac{\partial \zeta}{\partial x} + \underbrace{K \frac{\epsilon_0 \phi_0}{\delta_0}}_{\mathcal{D}_i} \frac{|u|u}{D} = 0. \tag{4}$$

These equations are controlled by three independent, external, dimensionless parameters: the dimensionless tidal amplitude, also named nonlinearity parameter,

$$\epsilon_0 = \frac{A_0}{D_0},$$

the convergence ratio,

$$\delta_0 = \frac{L_{w0}}{L_{b0}},$$

and the friction parameter,

$$\phi_0 = \frac{C_{f0} L_{w0}}{D_0},$$

where $L_{w0} = (gD_0)^{1/2} \omega_0^{-1}$ is the frictionless tidal-wave length scale. The dimensionless velocity $K = \frac{U_0}{L_{b0} A_0 D_0^{-1} \omega_0}$ (also termed convergence parameter, Lanzoni and Seminara, 1998) and the dimensionless parameter $\mathcal{L} = \frac{L_0}{L_{b0}}$ are unknown functions of the 3 external dimensionless parameters: $\epsilon_0, \delta_0, \phi_0$. The fact that tide propagation in convergent estuaries is controlled by three parameters was already pointed out by several authors and in particular by Lanzoni and Seminara (1998). The dimensionless tidal amplitude ϵ_0 characterizes the nonlinear effects and δ_0 accounts for the effect of width convergence. The third parameter, ϕ_0, is related to friction effects. Other expressions for the friction parameter can be obtained by combining the three parameters ϵ_0, δ_0 and ϕ_0. For instance, the friction parameter proposed by Parker (1991) is $\phi_P = \frac{\phi_0}{\delta_0}$, the one by Toffolon et al. (2006) and Savenije et al. (2008) is $\chi = \epsilon_0 \phi_0$, and the one by Munchow and Garvine (1991) is $\phi_M = (\epsilon_0 \phi_0)^{-1/3}$. All these scaling approaches are, of course, equivalent but we will show in section 4 that our friction parameter definition is the most appropriate to classify estuaries in terms of tidal bore occurrence.

3. Database

To classify alluvial estuaries in terms of tidal bore occurrence we collected in the literature data on tidal and geometric properties of a large variety of regularly funnel-shaped estuaries. Twenty one estuaries are documented in this paper (see Table 1), eight being tidal-bore estuaries (TB estuaries) and thirteen non tidal-bore estuaries (NTB estuaries). We have not considered TB estuaries with complex morphologies such as the Sée/Mont Saint Michel estuary (Furgerot et al. (2013)) or the Petitcodiac estuary (Bartsch-Winkler and Lynch (1988)). It is worth mentioning that the morphology of most estuaries presented in Table 2 is now constrained by man-made structures and cannot evolve naturally.

To analyze the effects of freshwater discharge, q_0, on tidal bore formation we use the field database collected during three long-term campaigns on the Gironde/Garonne estuary (Bonneton et al., 2011a, 2011b, 2012, 2015). These campaigns were the first to quantitatively characterize tidal bore formation and propagation in an estuary, over a long period of time and for a large range of tidal amplitudes and freshwater discharges. Field experiments were carried out in the Garonne River at Podensac (see Fig. 1), 126 km upstream from the river mouth. The first campaign, TBG1, was conducted around the spring equinox in 2010 for large q_0 and the two others, TBG2 and TBG3, around the autumn equinoxes in 2010 and 2011 for low q_0.

4. Estuarine classification

Tidal bores can form in estuaries when the tide is strongly nonlinear with a marked ebb-flood asymmetry (ebb duration longer than the flood and larger flood than ebb currents). This asymmetry is mainly controlled by the dissipative parameter $\mathcal{D}_i = \frac{K\epsilon_0 \phi_0}{\delta_0}$ (see Eq. (4)) which characterizes the relative intensity of

Table 1
Table of symbols.

Parameter	Description
$A_0 = Tr_0/2$	Tidal amplitude at the mouth
B	Channel width
B_0	Channel width at the mouth
C_{f0}	Characteristic friction coefficient
D	Cross-sectional averaged water depth
D_0	Characteristic water depth
D_1	Low-tide water depth
L_0	Characteristic horizontal length-scale
L_{b0}	Convergence length
$L_{w0} = (gD_0)^{1/2}\omega_0^{-1}$	
q_0	Freshwater discharge
T_0	Tidal period
Tr	Local tidal range
Tr_0	Tidal range at the mouth
u	Cross-sectional averaged velocity
U_0	Characteristic tidal velocity
ζ	Surface elevation
$\omega_0 = 2\pi/T_0$	Tidal angular frequency
$\delta_0 = L_{w0}/L_{b0}$	Convergence ratio
δ_c	Critical convergence
$\varepsilon = (Tr/2)/D_1$	Local tidal wave nonlinearity parameter
$\varepsilon_0 = A_0/D_0$	Tidal wave nonlinearity parameter at the mouth
ε_c	Critical nonlinearity parameter
$\phi_0 = C_{f0}L_{w0}/D_0$	Friction parameter
$\chi = \varepsilon_0\phi_0$	Toffolon et al. (2006) friction parameter
$\mathcal{D}_i$	Dissipative parameter
Fr	Bore Froude number
K	Convergence parameter
$\mathcal{L} = L_0/L_{b0}$	
$\mathcal{Q}_0 = q_0/(A_0B_0L_{b0}\omega_0)$	Dimensionless river discharge

nonlinear frictional effects (see Lanzoni and Seminara (1998)). Bonneton et al. (2015) showed that tidal bores can form when the dissipative parameter is sufficiently large. This condition is a necessary but not a sufficient one.

In this section we analyze tidal bore occurrence as a function of

Table 2
Tidal and geometric properties of convergent alluvial estuaries. D_0, water depth; L_{b0}, convergence length; A_0, mean spring tidal amplitude at the estuary mouth; C_{f0}, friction coefficient. Sources: 1, 4, 11, 13, 14, 18, 20, data from Savenije (2012); 2, 3, 6, 7, 15, 19, 21, data from Lanzoni and Seminara (1998); 8, 9, 10, 16, 17, data from Bonneton et al. (2015) where we substituted the mean spring tidal amplitude for the maximum spring tidal amplitude; 5, data from Wolanski et al. (2006); 12, data from Winterwerp et al. (2013). We consider that for these 21 estuaries the dominant tidal period T_0 is semi-diurnal.

|	Estuaries	Tidal bore	D_0 (m)	L_{b0} (km)	A_0 (m)	C_{f0}
1	Chao Phya	No	7.2	109.	1.2	0.0039
2	Columbia	No	10.	25.	1.0	0.0031
3	Conwy	No	3.	6.3	2.4	0.0051
4	Corantijin	No	6.5	48.	1.0	0.0032
5	Daly	Yes	10.	27.	3.0	0.0025
6	Delaware	No	5.8	40.	0.64	0.0021
7	Elbe	No	10.	42.	2.0	0.0025
8	Gironde	Yes	10.	43.	2.3	0.0025
9	Hooghly	Yes	6.	25.	2.15	0.0015
10	Humber	Yes	12.	25.	3.2	0.0031
11	Limpopo	No	7.	50.	0.55	0.0027
12	Loire	No	13.	21.	2.5	0.0024
13	Mae Klong	No	5.2	155.	1.0	0.0035
14	Maputo	No	3.6	16.	1.4	0.0027
15	Ord	Yes	4.	15.2	2.5	0.0024
16	Pungue	Yes	4.	17.	3.2	0.0031
17	Qiantang	Yes	10.	40.	3.1	0.0015
18	Scheldt	No	10.5	28.	2.0	0.0023
19	Severn	Yes	15	41.	3.0	0.0025
20	Tha Chin	No	5.3	87.	1.35	0.0048
21	Thames	No	8.5	25.	2.0	0.0050
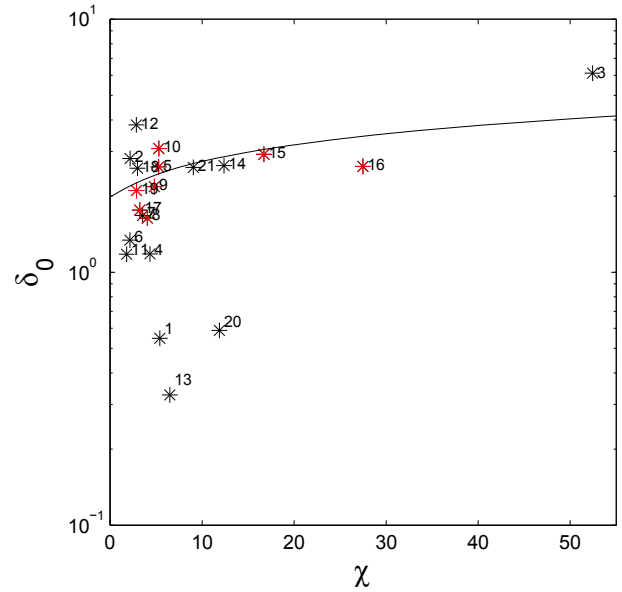
Fig. 3. Position of convergent alluvial estuaries (see Table 1) in the parameter plane ($\times$, δ_0). Red and black asterisks correspond to estuaries with and without tidal bore respectively. Continuous line: critical convergence δ_c from Eq. (5).

the three external dimensionless parameters (ε_0, δ_0, ϕ_0). Fig. 2 presents the positions, in the three-dimensional parameter space, of the 21 estuaries introduced in section 3. The projection on the plane (ε_0, δ_0) is plotted in Fig. 2a. In this plane there is no clear separation between TB and NTB estuaries. We can note that large dimensionless tidal amplitudes correspond to large estuary convergences. This observation, which points to a coupling between the forcing tide and the estuary morphology, is in agreement with previous results by Prandle (2003) for UK and US estuaries and Davies and Woodroffe (2010) for North Australian estuaries. The eight TB estuaries listed in Table 1 are characterized by large δ_0 values with a relatively low dispersion around the mean value of 2.4. It is worth mentioning that these convergence ratios are close
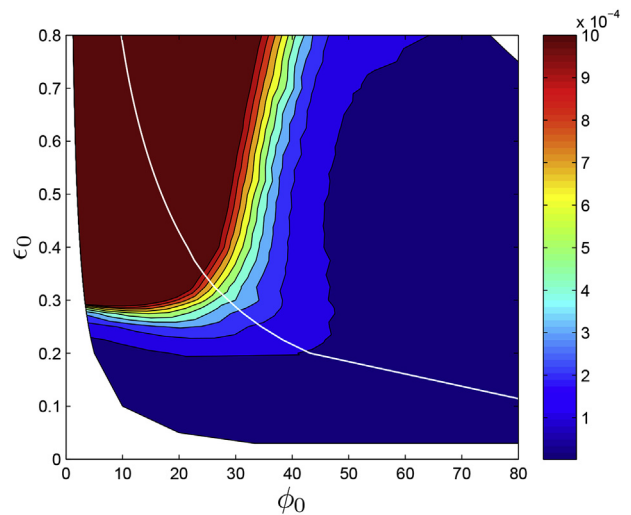

Fig. 4. Maximum slope of the tidal wave at $x = 3L_{b0}$; the colormap is limited to slope values bellow 10^{-3}, a value above where we consider TB occurring; each point in the plane (ϕ_0, ε_0) represents the numerical tidal wave solution for an idealized convergent estuary of constant convergent parameter: $\delta_0 = 2$; this figure relies on 225 numerical simulations (Arpaia et al. (2015)); white line, zero-amplification curve.

to the critical convergence δ_c introduced by Jay (1991) and Savenije et al. (2008). δ_c is a threshold condition for the transition from the mixed tidal wave to the "apparent standing" wave. Savenije et al. (2008) derived an equation relating the critical convergence and the dimensionless parameter $\chi = \varepsilon_0 \phi_0$. This relation is as follows:

$$\chi(\delta_c) = \frac{1}{2}\delta_c\left(\delta_c^2 - 4\right) + \frac{\left(\delta_c^2 - 2\right)}{2}\sqrt{\delta_c^2 - 4}. \qquad (5)$$

The positions of the 21 estuaries in the plane (δ_0, χ) are plotted in Fig. 3. We can see in this figure that tidal bores occur near critical convergence. At this stage we have no physical explanation for this observation and further theoretical or numerical investigations would be desirable.

Considering that $K \simeq 1$ (see Bonneton et al. (2015)) and that δ_0 is nearly constant, the dissipative parameter writes $\mathcal{D}_i = \alpha \varepsilon_0 \phi_0$, or using notations by Toffolon et al. (2006) $\mathcal{D}_i = \alpha \chi$, where α is a constant. Large values of $\mathcal{D}_i$ (or equivalently χ) correspond to high tidal wave asymmetry, favorable to tidal bore formation, but also to high energy dissipation leading to tidal damping which is unfavorable to tidal bore formation. By using the parameters (ϕ_0, ε_0) it is possible to distinguish between these two different effects. This is why we have introduced the new friction parameter ϕ_0 in this paper.

The projection on the plane (ϕ_0, ε_0) is plotted in Fig. 2b. In this parameter plane we can observe a clear separation between TB and NTB estuaries. Tidal bores occur when the nonlinearity parameter ε_0 is greater than a critical value, ε_c, which is an increasing function of ϕ_0. For small ϕ_0 values ($\phi_0 \sim 15$), corresponding to estuaries such as the Severn estuary, tidal bores can form for ε_0 greater than 0.2. By contrast, for large ϕ_0 values the tidal bore formation requires much larger nonlinearity parameters. For instance, in the Conwy estuary the tidal wave dynamics is strongly nonlinear ($\varepsilon_0 = 0.8$), but its very large friction parameter value ($\phi_0 = 65$) prevents tidal bore formation.

Due to the limited number of estuaries documented in this paper it is difficult to accurately characterize the function $\varepsilon_c(\phi_0)$. To overcome this experimental limitation we have used a 2D Saint Venant model to compute tidal wave solutions for 225 positions in the parameter plane (ϕ_0, ε_0). We have performed our simulations using the shock-capturing shallow-water solver discussed and validated in Ricchiuto (2015). We consider idealized estuaries with a constant water depth, an exponentially decreasing width, a rectangular cross-sectional shape and a constant δ_0-parameter value ($\delta_0 = 2$). A detailed presentation and analysis of our numerical results can be found in Arpaia et al. (2015). From these numerical simulations, we analyze tidal bore occurrence by determining the maximum elevation slope of the tidal wave, $\alpha_m = \max(\partial\zeta/\partial x)$, for each position in the parameter plane (ϕ_0, ε_0). On the basis of field measurements by Bonneton et al. (2015), we consider that a tidal bore is formed when the maximum elevation slope α_m is larger than 10^{-3}. Fig. 4 presents the evolution of α_m in the parameter plane (ϕ_0, ε_0). We observe in this figure a separation between TB and NTB estuaries, which is in qualitative agreement with real-estuary observations (see Fig. 2b). In Fig. 4 the critical curve, $\varepsilon_c(\phi_0)$, differs slightly from that of Fig. 2b. This is due to the simplifying modeling assumptions and in particular the hypotheses of constant δ_0 and constant water-depth. In real alluvial estuaries it is common to observe a decreasing water depth in the upper estuary. Such a condition is favorable to tidal bore formation and can explain why the critical curve for real estuaries (Fig. 2b) is located slightly below that of idealized constant-depth estuaries (Fig. 4).

The white curve in Fig. 4 shows the position of estuaries for which tidal amplification, $\delta_A = \frac{1}{T_r}\frac{dT_r}{dx}$, is equal to zero. These estuaries are named ideal estuaries or synchronous estuaries (see

Savenije (2012)). The region below this curve corresponds to amplified estuaries (also named hypersynchronous estuaries) while the region above it corresponds to damped estuaries (also named hyposynchronous estuaries). Arpaia et al. (2015) showed that this zero-amplification curve, obtained from numerical simulations, is in close agreement with the theoretical law derived by Savenije et al. (2008) (their equation (61)), for the selected value of $\delta_0 = 2$. It is generally accepted that tidal bores form in amplified estuaries (see Chanson (2012)). However, our numerical simulations show in Fig. 4 that the intersection between TB estuaries and damped estuaries is not empty. This intersection corresponds to the region, in the parameter plane (ϕ_0, ε_0), located above both the zero-amplification curve and the ε_c critical curve. Two real estuaries, the Ord and Pungue, can be identified in this region (see Fig. 2b). Both are TB estuaries associated with damped tidal waves, which confirm our modeling results. Other damped TB estuaries have been documented in the literature, such as the Seine estuary ((Bonneton et al., 2012, 2015)) or the Sée and Sélune rivers (Furgerot (2014)).[1] These observations along with our modeling approach, show that tidal wave amplification is clearly not a necessary condition for tidal bore formation.

5. Freshwater discharge effects

In the preceding section we considered tidal bore formation under the most favorable conditions (spring tides and low q_0) which allowed us to neglect freshwater discharge effects in our analysis. However, it is well known that tides in estuaries may be significantly affected by the rate of discharge (e.g. Parker (1991) or Horrevoets et al. (2004)), especially in the upper estuary, where tidal bores generally occur.

In this section we analyze the effect of freshwater discharge on tidal bore formation, on the basis of 3 Gironde/Garonne field campaigns covering a large range of tidal amplitudes A_0 and
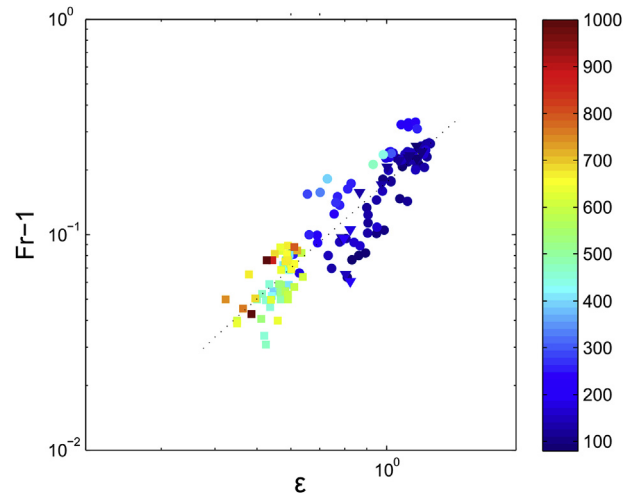

Fig. 5. Evolution of the tidal bore Froude number, Fr, minus 1, as a function of the nondimensional local tidal amplitude $\varepsilon = \frac{Tr/2}{D_1}$, where D_1 is the water depth at low tide. Observations were performed in the upper Gironde/Garonne estuary at Podensac ($x = 126$ km $\simeq 3L_{b0}$); the colormap shows the freshwater discharge, q_0, in m³/s; square symbol, TBG1 campaign; circle symbol, TBG2 campaign; triangle symbol, TBG3 campaign; Dotted line, linear fit.

---

[1] These three TB estuaries have not been included in our scaling analysis (Table 1) because of the complexity of their morphological shape which cannot be described by one convergence length L_{b0}.
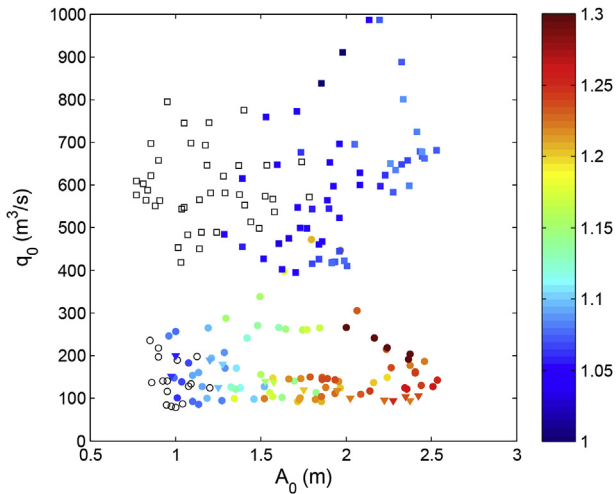
Fig. 6. Position of the tides, observed during 3 field campaigns on the Gironde/Garonne estuary, in the plane (A_0, q_0). Close and open symbols correspond to tidal wave with and without tidal bore respectively; square symbol, TBG1 campaign; circle symbol, TBG2 campaign; triangle symbol, TBG3 campaign; the colormap shows the tidal bore Froude number.

freshwater discharges q_0. Field measurements were carried out in the upper estuary at 126 km upstream of the river mouth. Bonneton et al. (2015) showed that tidal bore occurrence and intensity are mainly governed by the local dimensionless amplitude, $\varepsilon = \frac{Tr/2}{D_1}$, where Tr is the field site tidal range and D_1 is the water depth at low tide. This is confirmed by Fig. 5 which shows a close relation between the tidal bore Froude number[2] and ε. We do not observe in this figure any significant influence of freshwater discharge on the relation between Fr and ε. Indeed, a given dimensionless amplitude corresponds to a given Fr, whatever the value of q_0. This does not mean that tidal bore formation is independent on q_0 because the ε parameter, which characterizes the tidal wave nonlinearity, is strongly dependent on q_0. Indeed, D_1 and Tr are respectively increasing and decreasing functions of q_0 (see Bonneton et al. (2015)), and hence ε is a decreasing function of q_0.

For a given estuary (herein the Gironde/Garonne estuary) the two main external variables controlling tidal waves are A_0 and q_0. Fig. 6 presents the occurrence and intensity of tidal bores, in the plane (A_0, q_0), for all tides observed during our 3 field campaigns on the Gironde/Garonne estuary. In contrast to the preceding sections, we do not restrict our analysis to spring tides and we consider the whole range of tidal wave amplitudes A_0, from neap to spring tides. Fig. 6 shows that the tidal bore intensity (estimated from the Froude number) is an increasing function of A_0 and a decreasing function of q_0. The freshwater discharge plays a damping role on the tidal wave as it propagates along the estuary. Cai et al. (2014) showed, from an analytical mathematical approach, that this process is essentially due to the fact that the river discharge increases the friction term. For large q_0 ($q_0 \simeq 1000$ m³/s), and then strong friction-damping effects, tidal bores rarely occur. However, low-intensity tidal bore can eventually form during spring tides (see Fig. 6). By contrast, for low q_0, the tidal wave is amplified and tidal bores can even form at neap tide ($A_0 = 0.95$). In Fig. 6 we do not observe a sharp transition between tidal-bore and non tidal-bore regimes. This indicates that tidal bore occurrence can also depend on secondary external variables such as wind intensity and direction, atmospheric pressure and non stationarity of the freshwater discharge.

To take into account the freshwater discharge in the tidal-bore scaling analysis it is necessary to introduce a fourth external parameter. This fourth parameter is the dimensionless river discharge $\mathcal{Q}_0$, which characterizes the ratio between the freshwater discharge and the tidal discharge at the estuary mouth (see Cai et al. (2014)). In order to express $\mathcal{Q}_0$ as a function of the external variables of the problem, we take for the characteristic velocity scale $U_0 = L_{b0}A_0D_0^{-1}\omega_0$ (i.e. $K=1$). Hence $\mathcal{Q}_0$ is written:

$$\mathcal{Q}_0 = \frac{q_0}{A_0 B_0 L_{b0} \omega_0}$$

where B_0 is the characteristic channel width at the estuary mouth[3]

6. Conclusion

We have presented in this paper the first quantitative study of the conditions for tidal bore formation in convergent alluvial estuaries. First, we have shown that TB estuaries are characterized by large convergence ratios which are close to the critical convergence δ_c. To classify alluvial estuaries in terms of tidal bore occurrence we have introduced a new dimensionless friction parameter $\phi_0 = \frac{C_{f0}L_{w0}}{D_0}$. By exploring the parameter space (ϕ_0, ε_0), from both field data and numerical simulations, we have shown that tidal bores form in convergent estuaries when the nonlinearity parameter ε_0 is greater than a critical value ε_c. This critical nonlinearity parameter is an increasing function of the friction parameter ϕ_0. We have also identified a region in the parameter space (ϕ_0, ε_0) which corresponds to TB estuaries with damped tidal waves. This new result shows that, contrary to what is generally assumed, tide amplification is not a necessary condition for tidal bore formation.

We have also analyzed flow conditions for which the freshwater discharge can no longer be neglected. In this context, it is necessary to introduce a fourth external parameter, the dimensionless river discharge $\mathcal{Q}_0 = \frac{q_0}{A_0 B_0 L_{b0} \omega_0}$. We have shown that in the upper estuary the tidal bore intensity is mainly governed by the local dimensionless tide amplitude ε. The bore intensity is an increasing function of ε and this relationship does not depend on freshwater discharge. However, freshwater discharge damps the tidal wave during its propagation and thus reduces ε and consequently limits the tidal bore development in the estuary.

In this paper we have introduced the main dimensionless parameters controlling tidal bore formation and propose, for the first time, an estuarine classification in terms of tidal bore occurrence. Our approach has been validated from both field observations and numerical simulations. However, tidal bore observation worldwide are most often qualitative and usually based on visual observations (e.g. (Lynch, 1982; Bartsch-Winkler and Lynch, 1988; Chanson, 2012)). An accurate estuarine classification would require new quantitative field measurements, like those of (Simpson et al., 2004; Wolanski et al., 2004; Uncles et al., 2006; Bonneton et al., 2011a, 2012, 2015; Chanson et al., 2011; Furgerot et al., 2013), for estuaries having contrasting characteristics. Furthermore, addressing alluvial estuaries with nonlinearity parameter ε_0 close to $\varepsilon_c(\phi)$ would allow a more accurate determination of the critical curve between TB and NTB estuaries. In parallel with these new observations it would also be important to extend the scaling analysis presented in this paper, particularly taking into account large-scale spatial variations of the estuary water depth.

---

[2] The Froude number is computed from the relation $Fr = \frac{|u_1 - c_b|}{(gD1)^{1/2}}$, where c_b is the bore celerity and u_1 and D_1 are the cross-sectionally averaged velocity and water depth ahead of the bore.

[3] This dimensionless river discharge parameter $\mathcal{Q}_0$ is closely linked to the Canter-Cremers number (see *Savenije* (2012), section 2.3).

Acknowledgments

References

Arpaia, L., Filippini, A., Bonneton, P., Ricchiuto, M., 2015. Modelling analysis of tidal bore formation in convergent estuaries. Submitt. Ocean Model.

Bartsch-Winkler, S., Lynch, D.K., 1988. Catalog of Worldwide Tidal Bore Occurrences and Characteristics. US Government Printing Office.

Bonneton, P., Van de Loock, J., Parisot, J.-P., Bonneton, N., Sottolichio, A., Detandt, G., Castelle, B., Marieu, V., Pochon, N., 2011a. On the occurrence of tidal bores — the Garonne River case. J. Coast. Res. SI 64, 11462—11466.

Bonneton, P., Barthelemy, E., Chazel, F., Cienfuegos, R., Lannes, D., Marche, F., Tissier, M., 2011b. Recent advances in SerreGreen Naghdi modelling for wave transformation, breaking and runup processes. Eur. J. Mech. B Fluids 30 (6), 589—597.

Bonneton, N., Bonneton, P., Parisot, J.-P., Sottolichio, A., Detandt, G., 2012. Tidal bore and Mascaret — example of Garonne and Seine Rivers. Comptes Rendus Geosci. 344, 508—515.

Bonneton, P., Bonneton, N., Parisot, J.P., Castelle, B., 2015. Tidal bore dynamics in funnel-shaped estuaries. J. Geophys. Res. Oceans 120 (2), 923—941.

Cai, H., Savenije, H.H.G., Jiang, C., 2014. Analytical approach for predicting fresh water discharge in an estuary based on tidal water level observations. Hydrology Earth Syst. Sci. 18 (10), 2014.

Chanson, H., Reungoat, D., Simon, B., Lubin, P., 2011. High-frequency turbulence and suspended sediment concentration measurements in the Garonne River tidal bore. Estuar. Coast. Shelf Sci. 95 (2), 298—306.

Chanson, H., 2012. Tidal Bores, Aegir, Eagre, Mascaret, Pororoca: Theory and Observations. World Scientific, Singapore.

Davies, G., Woodroffe, C.D., 2010. Tidal estuary width convergence: Theory and form in North Australian estuaries. Earth Surf. Process. Landforms 35, 737749. http://dx.doi.org/10.1002/esp.1864.

Friedrichs, C.T., Aubrey, D.G., 1994. Tidal propagation in strongly convergent channels. J. Geophys. Res. 99 (C2) http://dx.doi.org/10.1029/93JC03219, 33213336.

Friedrichs, C.T., 2010. Barotropic tides in channelized estuaries. Contemp. Issues Estuar. Phys. 27—61.

Furgerot, L., Mouaze, D., Tessier, B., Perez, L., Haquin, S., 2013. Suspended sediment concentration in relation to the passage of a tidal bore (See River estuary, Mont Saint Michel Bay, NW France). In: Bonneton, P., Garlan, T. (Eds.), Proc. Coastal Dyn. 2013, pp. 671—682.

Furgerot, L., 2014. Propriétés hydrodynamiques du mascaret et de son influence sur la dynamique sédimentaire Une approche couplée en canal et in situ (estuaire de la Sée, Baie du Mont Saint Michel). University of Caen. Doctoral dissertation.

Horrevoets, A.C., Savenije, H.H.G., Schuurman, J.N., Graas, S., 2004. (2008), the influence of river discharge on tidal damping in alluvial estuaries. J. Hydrol. 294 (4), 213—228.

Jay, D.A., 1991. Green's law revisited: tidal long-wave propagation in channels with strong topography. J. Geophys. Res. Oceans 96 (C11), 20585—20598.

Lanzoni, S., Seminara, G., 1998. On tide propagation in convergent estuaries. J. Geophys. Res. 103 (C13) http://dx.doi.org/10.1029/1998JC900015, 3079330812.

LeBlond, P.H., 1978. On tidal propagation in shallow rivers. J. Geophys. Res. 83 (C9) http://dx.doi.org/10.1029/JC083iC09p04717, 47174721.

Lynch, D.K., 1982. Tidal bores. Sci. Am. 247, 146—156.

Munchow, A., Garvine, R.W., 1991. Nonlinear barotropic tides and bores in estuaries. Tellus A 43 (3), 246—256.

Parker, B.B., 1991. The relative importance of the various nonlinear mechanisms in a wide range of tidal interactions. In: Parker, B.B. (Ed.), Tidal Hydrodynamics. John Wiley, Hoboken, N. J, p. 237268.

Prandle, D., 2003. Relationships between tidal dynamics and bathymetry in strongly convergent estuaries. J. Phys. Oceanogr. 33 (12), 2738—2750.

Ricchiuto, M., 2015. An explicit residual based approach for shallow water flows. J. Comput. Phys. 280, 306—344.

Savenije, H.H.G., Toffolon, M., Haas, J., Veling, E.J.M., 2008. Analytical description of tidal dynamics in convergent estuaries. J. Geophys. Res. 113 http://dx.doi.org/10.1029/2007JC004408. C10025.

Savenije, H.H.G., 2012. Salinity and Tides in Alluvial Estuaries, 2nd revised edition, open access edition.

Simpson, J.H., Fisher, N.R., Wiles, P., 2004. Reynolds stress and TKE production in an estuary with a tidal bore. Estuar. Coast. Shelf Sci. 60 (4), 619—627.

Toffolon, M., Vignoli, G., Tubino, M., 2006. Relevant parameters and finite amplitude effects in estuarine hydrodynamics. J. Geophys. Res. 111 http://dx.doi.org/10.1029/2005JC003104. C10014.

Uncles, R.J., Stephens, J.A., Law, D.J., 2006. Turbidity maximum in the macrotidal, highly turbid Humber Estuary, UK: flocs, fluid mud, stationary suspensions and tidal bores. Estuar. Coast. Shelf Sci. 67, 30—52.

Winterwerp, J.C., Wang, Z.B., van Braeckel, A., van Holland, G., Kosters, F., 2013. Man-induced regime shifts in small estuariesII: a comparison of rivers. Ocean. Dyn. 63 (11—12), 1293—1306.

Wolanski, E., Williams, D., Spagnol, S., Chanson, H., 2004. Undular tidal bore dynamics in the Daly Estuary, Northern Australia. Estuar. Coast. Shelf Sci. 60 (4), 629—636.

Wolanski, E., Williams, D., Hanert, E., 2006. The sediment trapping efficiency of the macro-tidal Daly Estuary, tropical Australia. Estuar. Coast. Shelf Sci. 69 (1), 291—298.